RSC Advances

ROYAL SOCIETY OF CHEMISTRY

www.rsc.org/advances

Graphic for Manuscript

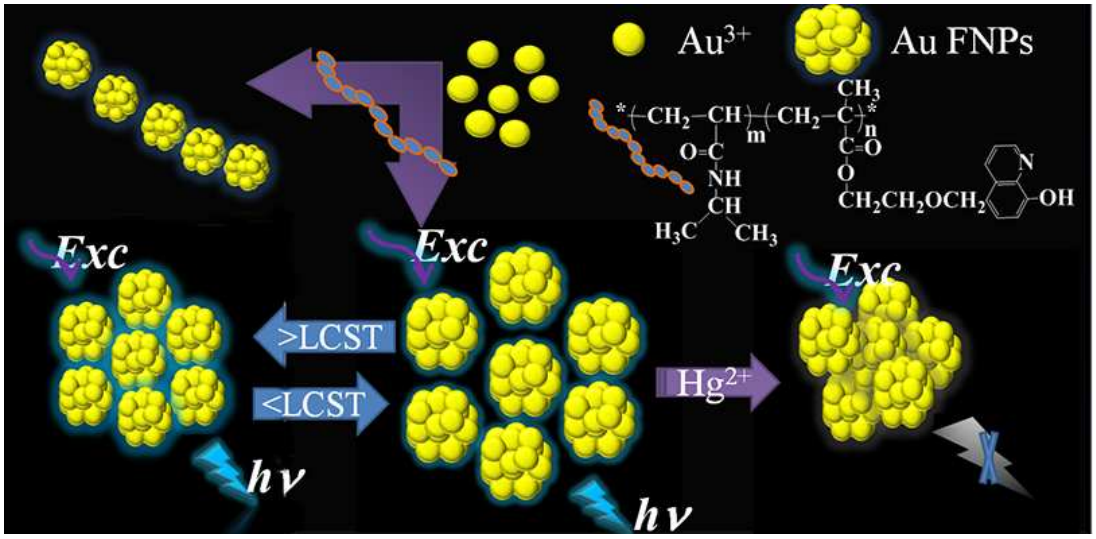

The novel thermosensitive copolymer ligand containing 8-hydroxyquinoline was employed as scaffold to construct the blue light emitting gold nanoparticles. These nanoparticles show interesting assemblies from nano-chains to nano-aggregates. The low cytotoxicity and detectable changes in luminescence make Au FNPs system excellent candidates for in vitro researches of the imaging and selective fluorescent sensing for Hg^{2+}.

Cite this: DOI: 10.1039/c0xx00000x

www.rsc.org/xxxxxx

ARTICLE TYPE

Blue light emitting gold nanoparticles functionalized with non-thiolate thermosensitive polymer ligand: optical properties, assemblies and application

Bingxin Liu, Yue Wang, Mingxiao Deng*, Jianhua Lü, Cuiyan Tong and Changli Lü*

Received (in XXX, XXX) Xth XXXXXXXXX 20XX, Accepted Xth XXXXXXXXX 20XX
DOI: 10.1039/b000000x

The thermoresponsive copolymer ligand containing 8-hydroxyquinoline capped gold NPs with blue light emission show the coordinate induced self-assemblies, aggregation-induced emission enhancement and sensitive detection to Hg^{2+} in aqueous solution with a detection limit of 0.9 nM.

Fluorescent gold nanoparticles (FNPs) or nanoclusters (NCs) have received considerable attention due to their intriguing molecular-like properties, such as the discrete electronic states and strong luminescence, ultra-small size, excellent photostability, and high sensitivity to their environment.[1] The emission center of gold clusters is usually assigned to the interband transition Au $5d^{10}$ to 6sp and/or ligand–metal charge transfer transition.[2] However, several issues fundamental to the luminescence of Au NCs, such as the source of emission (whether it is from Au atoms in the core or on the NC surface), the size effect in luminescence, and the critical factors in QY, are still presently not well understood. Several groups have studied the origin of the fluorescence of NCs and found that the surface of Au NCs plays a major role in fluorescence generation.[3] Since the development of thiolate gold nanoclusters, a large number of clusters have been prepared with different scaffolds, such as thiols,[4] dendrimers,[5] DNA[6] and proteins[7]. Thiolates has been widely used in the preparation of ligand-protected gold nanoclusters due in part to the aurophilic interaction.[8] Wu and Jin demonstrated that the surface of $Au_{25}(SR)_{18}$ played a major role in enhancing the fluorescence of Au NCs.[9] They found that the ligands with electron-rich atoms (e.g., N, O) or groups (e.g., COOH, NH_2) can largely promote fluorescence. Thus, the nature of the ligands used for capping the particle surface can markedly affect their emission properties.

To the best of our knowledge, there are few reports on the direct exploration of N-heterocyclic compounds with the important optoelectronic applications in the surface functionalization of Au NPs via coordinate bond.[10] It is known that 8-hydroxyquinoline (HQ) and its derivatives can coordinate the surface of semiconductor nanoparticles to form stable fluorescent complexes because these particles have a great number of surface metal atoms.[11] In this work, we utilized a copolymer ligand (CPL) containing HQ as capping agent to produce blue-light Au FNPs.

We have synthesized CPL-stabilized gold NPs by using three methods including both the "top-down" and the "bottom-up" approaches as shown in Scheme S1 (**ESI**†). 5-(2-methacryloylethyloxymethyl)-8-quinolinol (MQ) was selected as functional ligand to copolymerize with N-isopropylacrylamide (NIPAM) to fabricate a novel copolymer ligand (CPL). The number average molecular weight (M_n) of the copolymer was around 26000 with a polydispersity index (PDI) of 1.63. The CPL structure has been confirmed and the molar ratio of NIPAM and MQ units in CPL was calculated to be 58:1 by ^{1}H NMR in our previous work.[11b] The CPL exhibits a good solubility in aqueous solution with the lower critical solution temperature (LCST) of around 30 °C. Thus the CPL with electron donor group can be used as the ligand to *in situ* synthesize water-soluble Au NPs or decorate the surface of Au NPs via ligand exchange because the quinolinol units can anchor to the surface of Au NPs by coordinate bond.

The mild green reducing agent, *L*-ascorbic acid (*L*-Aa), also known as vitamin C, was utilized to produce the Au NPs (denoted as Au NPs-a hereafter). Generally, the growth of Au NPs-a strongly depended on the Au-to-ligand ratio, and the fluorescent Au NPs-a with a homogeneous size could be achieved only in the presence of excess ligands.[12] However, there is a reverse rule in our work when the Au NPs-a capped with CPL was synthesized in aqueous solutions with different Au/CPL ratios from 1:1 to 1:50 (Note: neither particles nor fluorescence was detected when the Au/CPL ratios were greater than 1:1). It is noteworthy from TEM images (Fig. S1 A to E) that the size of nanoparticles increases with increasing CPL dosage. The TEM images collected from different Au/CPL ratios for Au NPs a1 to a5 (the samples from a1 to a7 represent the CPL-capped Au NPs-a with the molar feed ratios of $[HAuCl_4]$/[CPL]=1:1, 1:5, 1:10, 1:20, 1:30, 1:40 and 1:50) show the homogeneous nanoparticles with average diameters of ca. 2.1, 4.5, 9.2, 19.1 and 28.3 nm, respectively. However, the nanoparticles of a6 and a7 were aggregated with broad dispersions. From the inset of Fig. S1F, the size dependence of Au NPs-a on Au/CPL ratios can be fitted with the binomial relationship (see ESI). Moreover, the well-resolved lattice planes of 0.24 nm spacing in the HRTEM image presents the crystalline structure of the resultant Au NPs-a (Fig. S1A).[13]

The crosscurrent is also supported by the UV–vis spectra in Fig. S2. The obvious broad surface plasma resonance (SPR) peak of

the Au NPs at 520 nm can be found when the Au/CPL ratios are greater than 1:5. The disappeared SPR absorption peak of the Au NPs a1 (Au/CPL=1:1) indicates that most of the particles are clusters. Because the small NPs no longer support the collective plasmon excitation due to the loss of metallic nature caused by quantum confinement effect.[14] The broad absorption of a6 and a7 at about 530 nm is responsible for the aggregated states of those Au NPs, which is in agreement with the result of TEM images. Fig. 1A shows the images collected under white light and UV irradiation for a set of Au NPs-a dispersions in water. The change in the dispersion color reflects the size effect of NPs on the plasmonic absorption. Fig. 1B also shows that the fluorescent intensity strongly depends on the Au-to-CPL ratio and the brightest emission at 475 nm is obtained for low Au/CPL ratios, such as 1:1 and 1:5. Through comparison with quinine (QY = 53%), the QY of the Au NPs a1 with Au/CPL ratio of 1:1 is 2.3%. Those samples of a3 and a4 with Au/CPL ratios less than 1:10 still show a weak fluorescence. Combining with the fluorescent Au NPs, we proposed that the blue luminescence should be attributed to the ligand-metal electronic transitions.

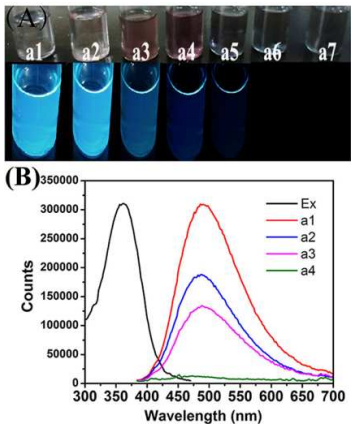

Fig. 1 (A) Digital images collected under daylight and UV irradiation for a set of Au NPs from a1 to a7 dispersions in water and (B) corresponding PL spectra of Au NPs a1 to a4.

The previous studies showed that the emission of Au NCs was tunable from ultraviolet to NIR region depending on the cluster size.[1] Because the electrons are confined in the nanoclusters with molecule-like discrete electronic energy levels, analogous to the Fermi wavelength of free electron (~0.7 nm). For those Au NCs which fluorescence orient from gold core, the increasing nanocluster size leads to lower energy emission.[15] However, our present work does not exhibit the similar size-dependent tunable emission of Au NPs-a. We can find from Fig. 1B that Au NPs-a possess different sizes but show same maximum emission wavelength at 475 nm. Namely, if the blue fluorescence is attributed to the intrinsic properties of the Au_8 cluster, the relative size of Au NPs should be less than 1 nm. But all of these Au NPs are bigger than 2 nm from the TEM images. Thus, we propose that the origin of blue light emission of CPL capped Au NPs should be a ligand-to-metal charge transfer transition. As predicted by previous work, luminescent Au NCs are expected to exhibit d and sp bands.[16] Since the sizes of Au NPs are around 2 nm, the energy level spacing within the sp band is too small to give visible emission.[17] Actually, the electronic structures of metals are not only dependent on their size but also strongly correlated with the oxidation state of metal atoms.[18] Since the HQ group is an electron donor ligand and its p orbital are higher in energy than the d orbitals of gold (I), the overlapping of these orbitals leads to the formation of ligand charge transfer excited states.[19]

The interaction between Au NPs and CPL was supported by UV-vis spectra (Fig. S2). The absorption signal at 259 nm for Au NPs@CPL is associated with the p–p* electron transition from quinoline ring. A new absorption band, which is caused by the N-to-gold charge transfer d–p* transition on the surface of Au NPs, can be observed at 370 nm, and the intensity of this signal increases with the increasing molar fraction of CPL. The above results indicate that an increasing amount of CPL ligands with MQ segments are anchored to the surface of Au NPs to form the metallo-quinolates. This result is also in agreement with our presumption that the luminescence is roughly attributed to quinoline-to-metal charge transfer transition.

To further prove the N-to-gold charge transfer, the mercaptoacetic acid (MPA) is expected to replace CPL since sulfur has a much higher affinity for gold than the HQ units of CPL. As shown in Fig. S3, this treatment completely eliminates the absorption peak at 370 nm of Au NPs@CPL and decreases the fluorescence intensity when the Au NPs a1 incubated in concentrated (0.5 M) MPA for 3 days. This intriguing finding provides the strong evidence that the original absorption peak at 370 nm arises from the ligand-metal charge-transfer transitions, and is related to the fluorescent properties of the Au NPs. Besides, the large Stokes shifts (144 nm) also suggest that the emission should result from a ligand-to-metal charge transfer transition.[20]

XPS measurements were performed to reveal the valence states of fluorescent gold NPs. As shown in Fig. 2, the binding energy (BE) for Au $4f_{7/2}$ of the Au NPs is 84.1 eV, which falls in the middle between Au (0) BE (83.9 eV) and Au(I) BE (85.1 eV), suggesting the coexistence of Au(I) and Au(0) in the Au NPs.[17] The Au 4f spectrum of the luminescent Au NPs can be deconvoluted into Au(I) and Au(0) components with binding energies of 84.3 and 85.1 eV, which are assigned to Au(0) and Au(I), respectively. On the basis of the area ratio between these two peaks, approximately 19% of the Au is on the surface of the Au FNPs as Au(I).

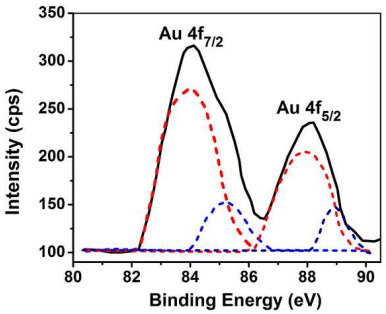

Fig. 2 XPS spectra of Au NPs b2 before (black line) and after deconvolution (red and blue line).

However, the fluorescent signal of Au NPs a1 can be only detected after 24h under vigorous stirring when *L*-Aa is used as reducing agent. A rapid approach for the synthesis of fluorescent Au NPs (denoted as Au NPs-b hereafter) was further developed by replacing *L*-Aa to alkali. Intense blue emission at 475 nm can

be observed immediately with the addition of ammonia solution by adjusting pH values from 7 to 10 (see Fig. S4). The brightest emission was detected at pH=9, which fluorescent intensity is about three times than that of Au NPs a1. The QY of Au NPs-b obtained from Au/CPL ratio of 1:5 can reach to 7 % at pH=9. Sun's work demonstrated the tendency of Au^{3+} to be reduced to Au^{0} or Au^{1+} was significantly increased at basic pH. [21] The formation of Au NPs-b could be regarded as the reverse reaction of the dissolution of the gold in aqua regia.[21] The as-prepared Au NPs prepared at pH=9 with different molar feed ratios are uniform in size (average size of 2 nm) and show interesting CPL induced self-assemblies (Fig.3). The Au NPs-chains assembly can be observed in Fig. 3A when the [Au^{3+}]/[CPL] is 1:1 (refered as b1). With increasing CPL dosage ([Au^{3+}]/[CPL] is 1:5, refered as b2), it is noteworthy that the separated Au NP nano-aggregates are mainly formed for Au b2.

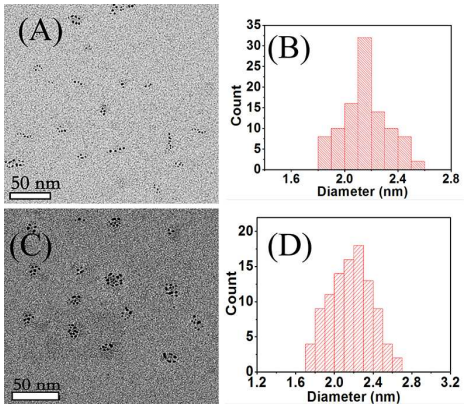

Fig. 3 TEM images and size distribution histograms of Au NPs-b with Au/CPL ratios of (A, B) 1:1 and (C, D) 1:5.

As mentioned above, the Au NPs-a reduced by *L*-ascorbic acid did not show any self-assembly structure which may attributed to the slow growth dynamics. As the fluorescence of the NPs (e.g. NPs-a1) only can be detected under vigorous stirring after 24 h, we assumed that less CPL dosage is not enough to support big and stable particles. Thus these big NPs will adjust the size via a CPL induced etching process until form stable FNPs. This assumption is in accordance with the reverse rule of NPs-a that the NPs size depend on the Au-to-ligand ratio. However, the alkali induced NPs-b processed a rapid growth dynamics which lead to form stable CPL capped NPs. Therefore, the CPL can bind to different Au NPs which are thus interconnected and a self-assembly structure is formed. For CPL with multiple HQ groups, there are two reasonable binding schemes that could exist between Au NPs and CPL due to the stable coordinate bond between the CPL and the gold atoms on the NPs surface: (i) the copolymers could be linked to the same Au NPs' surfaces at multiple sites. The Au NPs-a system may form monodispersed NPs in such case. (ii) the CPL could connect to different Au NPs by their binding groups of HQ units, which are thus interconnected and a chain or network is formed (Scheme 1). From the TEM images, a possible coordination structure resulting from the bridging of neighboring Au NPs-b induced by CPL chains and the copolymers connecting with their binding groups to different Au NPs is supposed.

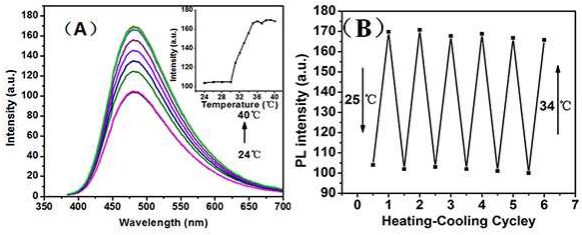

Fig. 4 (A) PL spectra of Au NPs-b2 at different temperatures and (B) Heating–cooling cycles of Au NP-b2 at above and below the LCST.

As the CPL has the sensitive thermally triggered response, the PL properties of copolymer ligand capped Au NPs-b at different temperatures are shown in Fig. 4. With rising temperature, a remarkable increase in the PL intensity of Au NPs-b2 was observed. The PL intensity is almost unchanged when the temperature is above 34°C. Thus, the aggregation of Au NPs-b2 assemblies caused by the volume transition of CPL networks upon heating may lead to the emission enhancement. It is noteworthy that only Au NPs-b2 shows the obvious aggregation-induced emission enhancement (AIEE), which may be assigned to the special crosslinking assemblies. Six cycles of heating–cooling were also performed and it was found that the temperature-responsive behavior of the Au NPs assemblies were highly reversible, as shown in Fig. 4B. As far as we know, it is the first time to report the temperature driving AIEE of Au NPs assemblies (Scheme 1).

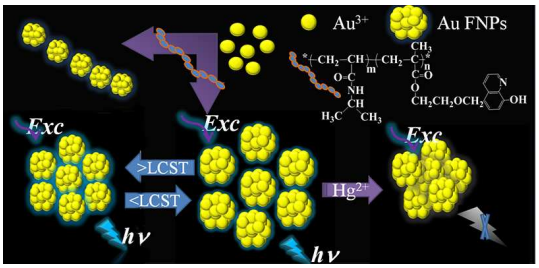

Scheme 1. Schematic illustration of the thermosensitive copolymer ligand functionalized Au FNPs assemblies. The assemblies show temperature driving aggregation-induced emission enhancement (AIEE) and selective detection of Hg^{2+}.

The etching-based strategy had also been used to synthesize fluorescent Au NPs and detailed discussion was shown in **ESI**. However, the decomposition kinetic is slow (at least several weeks at room temperature) as shown in Fig. S5 and S6 and follow-up handling is needed.

The fluorescent method based on Au NPs b2 for selective sensing of the Hg^{2+} was also constructed. It was found from Fig.5A that the fluorescence of the Au NPs b2 was efficiently quenched by the Hg^{2+} ions. The emission spectra displayed a gradual decrease in emission intensity with the increase in the solution Hg^{2+} concentration. There is a good linear relationship between fluorescence quenching and the logarithm of the Hg^{2+} concentration within the range of 10^{-9} to 10^{-4} M (Fig.5 B). The sensing system based on CPL capped Au FNPs can provide a limit of detection (LOD) to be 0.9 nM for Hg^{2+} ions (S/N = 3), which is comparable to that provided by 11-MUA-Au NCs[22], DHAL-Au NCs [23] and below the limit (10 nM) defined by the U.S. Environmental Protection Agency in drinkable water. This value of LOD is much lower than that from Lysozyme and

Trypsin capped Au NCs.[24] The selectivity of the Au NPs as a probe was tested by 14 other metal ions such as Ba^{2+}, Ca^{2+}, Cd^{2+}, Co^{2+}, Cr^{3+}, Cu^{2+}, Fe^{2+}, Fe^{3+}, K^{+}, Mg^{2+}, Mn^{2+}, Na^{+}, Ni^{2+}, and Pb^{2+} under the identical conditions (see Fig.5C). The result shows that only Hg^{2+} caused a pronounced fluorescence quenching, indicating that our Au NPs exhibit a high selectivity to Hg^{2+} over the competing metal ions. The typical TEM images (Fig.5D) show that Au NPs b2 are tend to form a compact crosslinked structure in the presence of Hg^{2+} ions. Therefore, we reasoned that Hg^{2+} may also be able to quench their fluorescence via the competitive coordinate interaction between Hg and Au with CPL because the CPL containing a nitrogen heterocyclic ring has the strong ability to bind with Hg^{2+} through coordination.

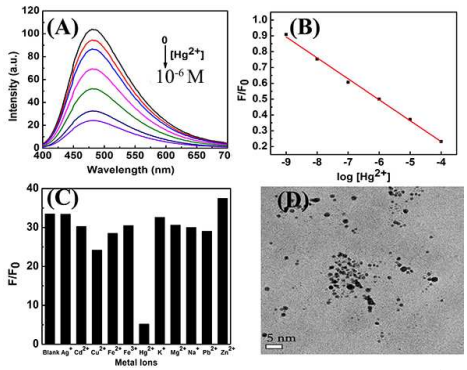

Fig. 5. (A) Fluorescence emission spectra of Au NPs-b2 at Hg^{2+} concentrations increasing from 0 to 10^{-6} M (top to bottom, excitation at 370 nm). (B) Relative fluorescence intensity of Au NPs-b2 (F/F_0, where F and F_0 are the fluorescence intensities at 475 nm in the presence and absence of Hg^{2+}, respectively) versus the logarithm of the Hg^{2+} concentration. (C) Fluorescence response of Au NPs (F/F_0) in the presence of different metal ions (all at 10 mM). (D) TEM image of Au NPs-b2 after addition of 10 mM Hg^{2+}.

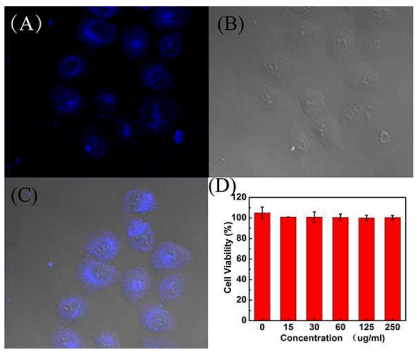

Fig.6. Confocal microscopic images of Hela treated with Au NPs-b2. The panels are (A) the luminescent image, (B) transmission image, and (C) an overlay, respectively. (D) Viability of HeLa cells after 24 h of incubation with different concentrations of Au NPs in the cell medium as determined by an MTT assay.

The novel Au NPs with low cytotoxicity were used in the in vitro researches of the imaging for human cervical cancer cells (HeLa, Fig.6). The bright field images and the overlay of fluorescence revealed that Au NPs were localized inside the HeLa cells (Fig.6B and C), demonstrating the capability of our Au NPs to stain the interior of living cells. The cytotoxicity of the CPL capped Au NPs was evaluated in HeLa cell lines that over express Tf receptors (Fig.6D). The results indicate that the Au NPs is generally low toxic for living cell, possibly due to good biocompatibility of the surrounded CPL with NIPAM units. The results indicate that the Au NPs is excellent candidates for in vitro researches of the imaging.

Conclusions

As conclusion, we deemed that the thermosensitive copolymer ligand played an important role in fabricating small blue-light Au NPs with the properties of self-assembly and AIEE, and the application of selective detection of Hg^{2+} and bioimaging. These novel multifunctional Au NPs are expected to find potential applications as optical sensors, devices, fluorescence labeling and disease therapy such as nanothermometers in a living cell.

Notes and references

Institute of Chemistry, Northeast Normal University, Changchun 130024, PR. China.
** Address correspondence to: lucl055@nenu.edu.cn; dengmx330@ nenu.edu.cn*

† Electronic Supplementary Information (ESI) available: Experimental details, TEM images, UV-vis and PL spectra. See DOI:10.1039/b000000x.

1 J. Zheng, P. R. Nicovich and R. M. Dickson, *Annu. Rev. Phys. Chem.*, 2007, **58**, 409.
2 X. L. Guével, B. Hötzer, G. Jungb and M. Schneider, *J. Mater. Chem.*, 2011, **21**, 2974.
3 M. Zhu, C. M. Aikens, F. J. Hollander, G. C. Schatz and R. Jin, *J. Am. Chem. Soc*., 2008, **130**, 5883.
4 L. Shang, N. Azadfar, F. Stockmar, W. Send, V. Trouillet, M. Bruns, D. Gerthsen and G. U. Nienhaus, *Small*, 2011, **7**, 2614.
5 J. Zheng, J. T. Petty and R. M. Dickson. *J. Am. Chem. Soc.*, 2003, **125**, 7780.
6 T. A. C. Kennedy, J. L. MacLean and J. Liu, *Chem. Commun.*, 2012, **48**, 6845.
7 J. Xie, Y. Zheng and J. Ying, *J. Am. Chem. Soc.*, 2009, **131**, 888.
8 L. Shang, S. Dong and G. U. Nienhaus, *Nano Today*, 2011, **6**, 401.
9 Z. Wu and R. Jin, *Nano Lett*., 2010, **10**, 2568.
10 (a) S. Kim and S. W. Joo, *Vib. Spectrosc.* 2005, **39**, 74; (b) M. Grzelczak, N. Kulisic, M. Prato and A. Mateo-Alonso, *Chem. Commun*., 2010, **46**, 9122.
11 (a) B. Liu, X. Lü, C. Tong, C. Wang, L. Feng, Y. He and C. Lü, *RSC Adv.*, 2013, **3**, 21298; (b) B. Liu, C. Tong, L. Feng, C. Wang, Y. He and C. Lü, *Macromol. Rapid Commun*., 2014, **35**, 77.
12 F. Aldeek, M. A. H. Muhammed, G. Palui, N. Zhan and H. Mattoussi, *ACS Nano*, 2013, **7**, 2509.
13 Y. Chen, X. Zheng, X. Wang, C. Wang, Y. Ding and X. Jiang, *ACS Macro Lett.*, 2014, **3**, 74.
14 Z. Wu, J. Suhan and R. Jin, *J. Mater. Chem.*, 2009, **19**, 622.
15 J. Zheng, C. W. Zhang and R. M. Dickson, *Phys. Rev. Lett.*, 2004, **93**, 077402.
16 R. L. White-Morris, M. M. Olmstead, F. L. Jiang, D. S. Tinti and A. L. Balch, *J. Am. Chem. Soc.*, 2002, **124**, 2327.
17 C. Zhou, C. Sun, M. Yu, Y. Qin, J. Wang, M. Kim and J. Zheng, *J. Phys. Chem. C*, 2010, **114**, 7727.
18 J. Zheng, C. Zhou, M. Yu and J. Liu, *Nanoscale*, 2012, **4**, 4073.
19 Y. Pei, Yi Gao, N. Shao and X. Zeng, *J. Am. Chem. Soc*., 2009, **131**, 13619.
20 V. W. W. Yam, E. C. C. Cheng and Z. Y. Zhou, *Angew. Chem. Int. Ed.*, 2000, **39**, 1683.
21 C. Sun, H. Yang, Y. Yuan, X. Tian, L. Wang, Y. Guo, L. Xu, J. Lei, N. Gao, G. J. Anderson, X. Liang, C. Chen, Y. Zhao and G. Nie, *J. Am. Chem. Soc.*, 2011, **133**, 8617.
22 C. C. Huang, Z. Yang, K. H. Lee and H. T. Chang, *Angew. Chem., Int. Ed.*, 2007, **46**, 6824.
23 L. Shang, L. X. Yang, F. Stockmar, R. Popescu, V. Trouillet, M. Bruns, D. Gerthsen and G. U. Nienhaus, *Nanoscale*, 2012, **4**, 4155
24 (a) Y. H. Lin and W. L. Tseng, *Anal. Chem.*, 2010, **82**, 9194; (b) H. Kawasaki, K. Yoshimura, K. Hamaguchi and R. Arakawa, *Anal. Sci.*, 2011, **27**, 591.